A Comparison Study of Normal-Incidence Acoustic Impedance Measurements of a Perforate Liner

Todd Schultz[1]
The Mathworks, Inc, Natick, MA 01760

Fei Liu,[2] Louis Cattafesta, Mark Sheplak[3]
University of Florida, Gainesville, FL 32611

and

Michael Jones[4]
NASA Langley Research Center, Hampton, VA 23681

The eduction of the acoustic impedance for liner configurations is fundamental to the reduction of noise from modern jet engines. Ultimately, this property must be measured accurately for use in analytical and numerical propagation models of aircraft engine noise. Thus any standardized measurement techniques must be validated by providing reliable and consistent results for different facilities and sample sizes. This paper compares normal-incidence acoustic impedance measurements using the two-microphone method of ten nominally identical individual liner samples from two facilities, namely 50.8 mm and 25.4 mm square waveguides at NASA Langley Research Center and the University of Florida, respectively. The liner chosen for this investigation is a simple single-degree-of-freedom perforate liner with resonance and anti-resonance frequencies near 1.1 kHz and 2.2 kHz, respectively. The results show that the ten measurements have the most variation around the anti-resonance frequency, where statistically significant differences exist between the averaged results from the two facilities. However, the sample-to-sample variation is comparable in magnitude to the predicted cross-sectional area-dependent cavity dissipation differences between facilities, providing evidence that the size of the present samples does not significantly influence the results away from anti-resonance.

I. Introduction

MODERN turbofan engines rely on acoustic liners to suppress engine noise and meet community noise standards. Noise suppression is accomplished by tailoring the acoustic impedance of the nacelle with acoustic liners designed to minimize the radiated acoustic energy from the engine [1]. Acoustic liner design requires experimental verification of the acoustic properties of candidate configurations. The two-microphone method (TMM) is a popular standardized technique for determining the normal-incidence specific acoustic impedance of liner samples [2-6] and offers rapid examination of candidate liner designs by comparing acoustic liner model predictions with experimental data. In this method, a compression driver is mounted at one end of an acoustic waveguide or normal-incidence impedance tube (NIT), and the test specimen is mounted at the other. Two microphones are flush-mounted in the duct wall at two locations near the specimen to determine the incident and reflected planar waves below the cut-on frequency for higher-order modes. The microphone data are used to estimate the complex reflection coefficient and corresponding acoustic impedance of the test specimen.

[1] Senior Application Engineer, 3 Apple Hill Drive, and Member AIAA.
[2] Post-Doctoral Associate, MAE Department, P.O. Box 116250, Member AIAA
[3] Professor, MAE Department, P.O. Box 116250, Associate Fellow AIAA
[4] Senior Research Scientist, Structural Acoustics Branch, Mail Stop 463, Associate Fellow AIAA

Whereas the uncertainty of the estimated acoustic impedance from the TMM has been studied in detail for individual liner samples in [7-12], this paper focuses on analysis of the measurements of several nominally identical specimens in two different facilities that use different specimen sizes. The two facilities have been shown to perform as expected for various canonical test specimens, such as sound hard rigid and anechoic terminations [11]. So this study provides the means to judge the effectiveness and reliability of the standard for more realistic test specimens and to assess the effects of sample size. Typically, the size of the sample is assumed to be large compared to any local irregularities in the material, and thus the specimen is assumed to be homogeneous.

The first facility is the normal-incidence impedance tube located in the Interdisciplinary Microsystems Group at the University of Florida (UF). This NIT has a cross-sectional area of 25.4 mm by 25.4 mm and a usable frequency range of 0.5 to 6.7 kHz. The second facility is the NIT at the Flow Impedance Test Laboratory at NASA Langley Research Center. This waveguide has a cross-sectional area of 50.8 mm by 50.8 mm and a usable frequency range of 0.3 to 3.0 kHz. Numerous measurements of multiple samples of a sample material are performed in each facility to permit statistical analysis of the measurement results and thereby distinguish between facility differences due to sample size and statistical sample-to-sample variations.
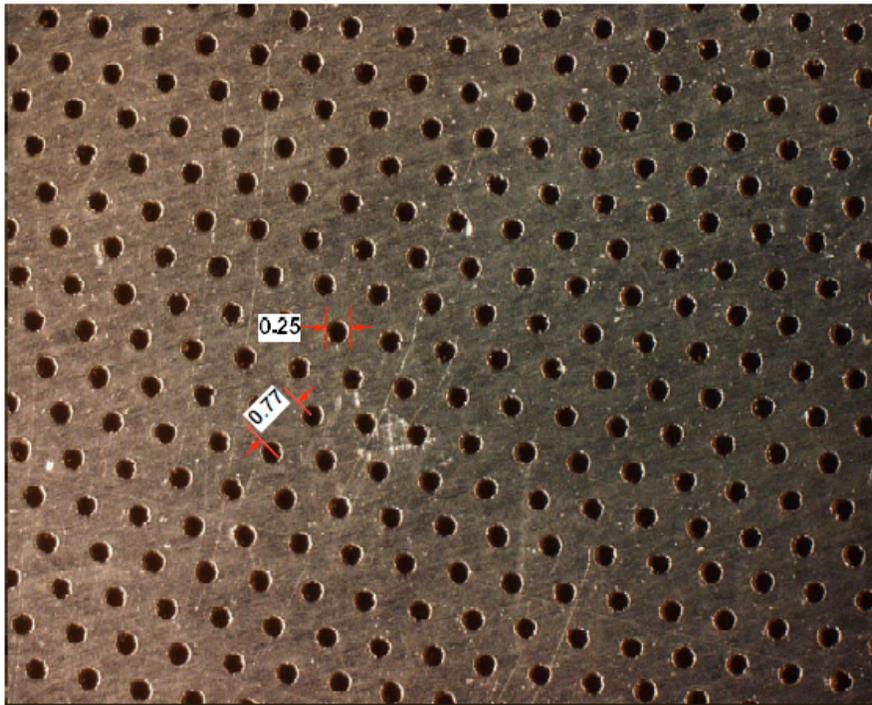
Figure 1. Schematic of the facesheet for the acoustic impedance provided by NASA Langley Research Center.

The sample chosen for this comparison study is a simple single degree-of-freedom liner supplied by NASA Langley Research Center. This sample configuration is well documented in the literature as a linear material, subject to limits on the incident sound pressure level, with analytical models of the acoustic impedance available for additional comparison [1]. The sample is composed of two parts: a 10% porous perforate facesheet, shown in Figure 1, and a resonator cavity. The holes of the 55.9 mm by 55.9 mm perforate facesheet were created via laser drilling with the entrance side (side irradiated by laser) of the hole facing the acoustic excitation source of the measurement apparatus. The nominal diameter of the holes is 0.254 mm and the nominal thickness of the facesheet is 1.27 mm. The depth of the resonator cavity is 76.2 mm. A custom sample holder was fabricated at UF so that the perforate facesheet was centrally mounted at one end of the UF NIT and the effective area of the sample was 25.4 mm by 25.4 mm. Similarly, a custom holder fabricated at NASA allowed the central 50.8 mm b 50.8 mm portion of the sample to be tested.

The paper is organized as follows. Section II briefly reviews the acoustic impedance model for a perforate facesheet backed with a resonator cavity. Nonlinearity of the acoustic impedance of the orifice at medium and high pressure level is considered. Section III describes the experimental methodology and facilities used at UF and

NASA. Experimental results and discussion are presented in Section IV, and conclusions and future work are provided in Section V.

II. Impedance Model

The acoustic impedance model of the orifice used in this paper is developed by combining Crandall's model [13], to compute the linear resistance and mass reactance of the orifice, with Melling's model [14], an impedance model for the orifice subject to medium-to-high pressure levels, to yield

$$\frac{Z_{\text{orifice}}}{\rho_0 c_0} = \frac{j\omega t}{c_0 \sigma \left[1 - \dfrac{2}{k_S a}\dfrac{J_1(k_S a)}{J_0(k_S a)}\right]} + \frac{16a\Psi\left(\sqrt{\sigma}\right)}{3\pi}\frac{j\omega}{c_0 \sigma \left[1 - \dfrac{2}{k_S a}\dfrac{J_1(k_S a)}{J_0(k_S a)}\right]} + \frac{1.2\left(1-\sigma^2\right)}{2c_0\left(\sigma C_D\right)^2}U ,$$

(1)

where ρ_0 is the air density, c_0 is the isentropic speed of sound, ω is the angular frequency, σ is the porosity of the perforate facesheet, a is the radius of the orifice, t is the thickness of the facesheet, $k_S = \sqrt{-j\rho_0\omega/\mu}$ is the Stokes wave number, μ is the coefficient of viscosity, U is the rms velocity through the orifice, and C_D is the discharge coefficient, which is dependent on the acoustic Reynolds number, $2\rho_0 Ua/\mu$. The typical value of the discharge coefficient is $C_D \approx 0.76$ [1]. The first term on the right hand side (RHS) of Eq. (1) is the same as the Crandall model and represents the linear impedance of the orifice. The second term on the RHS is the end correction, which also accounts for the interaction between the orifices via the Fok function [15]

$$\Psi\left(\sqrt{\sigma}\right) \approx 1 - 1.41\left(\sqrt{\sigma}\right) + 0.34\left(\sqrt{\sigma}\right)^3 + 0.07\left(\sqrt{\sigma}\right)^5 .$$

(2)

Notice that $\Psi\left(\sqrt{\sigma}\right)$ monotonically decreases with increasing porosity. When the porosity increases, the end correction of the mass reactance decreases. The third term on the RHS of Eq. (1) is the nonlinear resistance contribution applicable at medium-to-high sound pressure levels.

The perforate facesheet is backed with a resonator cavity with depth L. The specific acoustic impedance of the cavity is

$$\frac{Z_{cavity}}{\rho_0 c_0} = \coth\left(j\tilde{k}L\right),$$

(3)

where $\tilde{k} = \beta - j\alpha$ is the complex wave number, and α is the absorption coefficient which accounts for visco-thermal effects that lead to the absorption and dispersion of waves propagating inside the cavity and β is related to the phase speed of the sound [16]. Note that

$$\tilde{k} = \frac{\omega}{c_0}\left[1 + \frac{B}{2}\sqrt{\frac{\pi}{j\omega}}\right]$$

(4)

and

$$B = \frac{4}{d}\sqrt{\frac{\mu}{\pi\rho_0}}\left(1 + \frac{\gamma-1}{\sqrt{\text{Pr}}}\right),$$

(5)

where $d = 4S/C$ is the hydraulic diameter of the cavity, and S and C are the area and perimeter, respectively, of the cross section of the cavity, γ is the ratio of specific heats, and Pr is the Prandtl number. Combining Eqs. (4) and (5), we deduce

$$\alpha = \frac{2}{d}\sqrt{\frac{\omega\mu}{2\rho_0 c_0^2}}\left(1 + \frac{\gamma-1}{\sqrt{\text{Pr}}}\right).$$

(6)

Note that α varies as $1/d$, thus the cavity with different cross-section will cause different absorption of sound.

The specific acoustic impedance of the perforate facesheet with a resonator cavity is

$$\frac{Z_{IN}}{\rho_0 c_0} = \frac{Z_{orifice}}{\rho_0 c_0} + \frac{Z_{cavity}}{\rho_0 c_0}. \tag{7}$$

The root mean square velocity, U, through the orifice is thus given by

$$U = \left| \frac{10^{SPL/20} p_{ref}}{Z_1} \right|, \tag{8}$$

where p_{ref} is the reference pressure ($20 \mu Pa$). Combining Eqs.(1), (3), (6) and (7) gives the normalized specific acoustic impedance of the liner as a function of the sound pressure level measured at the facesheet

$$\frac{Z_{IN}}{\rho_0 c_0} = \frac{j\omega t}{c_0 \sigma \left[1 - \frac{2}{k_S a} \frac{J_1(k_S a)}{J_0(k_S a)} \right]} + \frac{16 a \Psi(\sqrt{\sigma})}{3\pi} \frac{j\omega}{c_0 \sigma \left[1 - \frac{2}{k_S a} \frac{J_1(k_S a)}{J_0(k_S a)} \right]} + \frac{1.2(1-\sigma^2)}{2c_0 (\sigma C_D)^2} \left| \frac{10^{SPL/20} p_{ref}}{Z_1} \right| + \coth(j\tilde{k}L). \tag{9}$$

However, the resulting equation is difficult to solve due to the nonlinearity. An iterative strategy is therefore implemented [17].

III.   Experimental Methodology

The data from both the UF NIT and the NASA NIT are acquired and reduced to normalized specific acoustic impedance values using the two-microphone method. To study the effects of sample size and sample variations, ten nominally identical samples are constructed and tested. These samples are tested in both facilities. The TMM and the analysis procedure of the multiple measurements are described in detail in this section.

A. Two-microphone Method

The TMM is a technique for estimating the normal specific acoustic impedance of a material and is defined by an ASTM standard, ASTM E1050-98 [2] and an ISO standard, ISO 10534-2:1998 [4]. The measurement consists of a sample mounted to one end of a NIT and a sound source at the other end. Two microphones are mounted flush to the side wall at two different axial locations and the acoustic pressures are recorded. The frequency response function is computed between the two microphones and the reflection coefficient is calculated, using a few other measurements such as the location of the microphones, the atmospheric temperature, by

$$R = \frac{\hat{H} - e^{-jks}}{e^{jks} - \hat{H}} e^{j2k(l+s)}, \tag{10}$$

where $\hat{H} = E\left[\hat{G}_{12}/\hat{G}_{11}\right]$ is the estimated complex frequency response function between Mic.1 and Mic.2. $E[\ ]$ is the expectation operator, $\hat{G}_{12}$ is the estimated cross spectrum between two microphones, and $\hat{G}_{11}$ is the estimated auto-spectrum of Mic.1. k is the wavenumber, s is the spacing between the microphone locations, and l is the distance from the sample to the nearest microphone location. The normalized specific acoustic impedance is then calculated by

$$\xi = \theta + j\chi = \frac{Z_1}{Z_0} = \frac{1+R}{1-R}, \tag{11}$$

where Z_1 is the measured specific acoustic impedance of the sample, Z_0 is the characteristic impedance of the medium, θ is the normalized resistance, and χ is the normalized reactance. For a complete description of the TMM, including frequency response function averaging, selection of microphone locations, etc. see references [2-4,8,9,11]. The experimental uncertainty estimate is computed using the procedure from Schultz et al. [12] only for the data from the UF NIT using a broadband excitation signal. An additional microphone is used in measurements in this study to measure the overall sound pressure level at the facesheet. This is done to ensure uniformity of testing conditions between the two facilities.
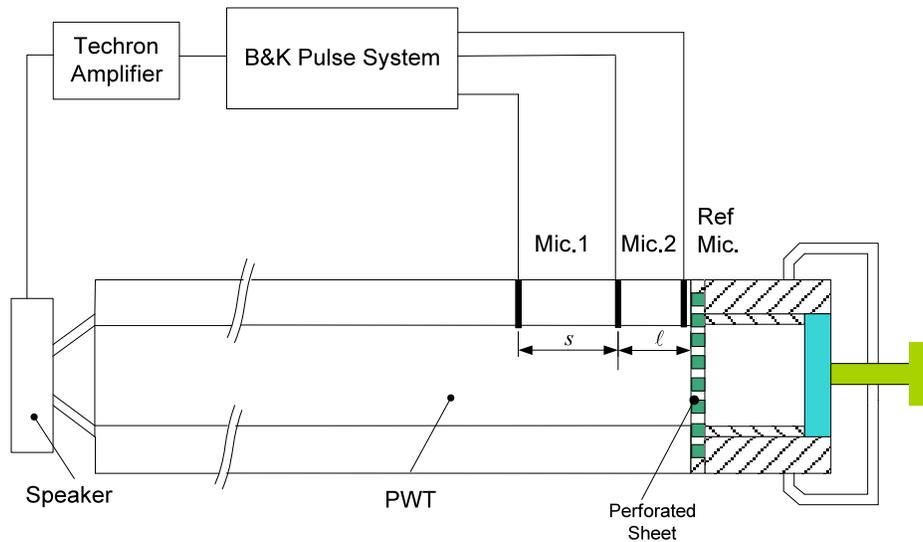
Figure 2. Schematic of the normal-incidence impedance tube at the University of Florida. Note that the schematic is not to scale.
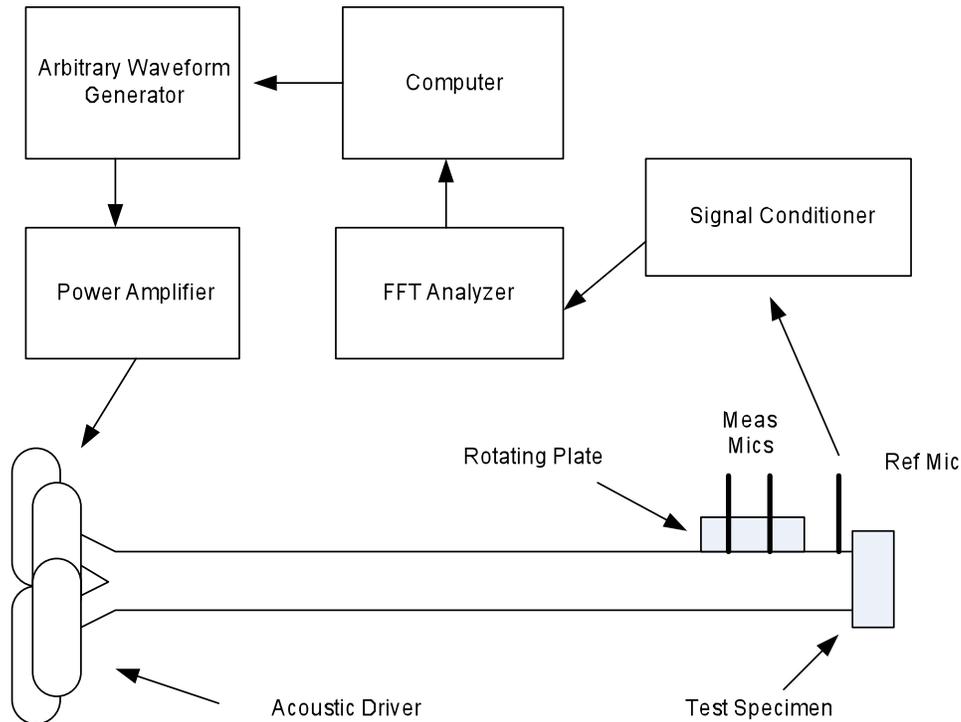
Figure 3. Schematic of the normal-incidence impedance tube at NASA Langley Research Center. Note that the schematic is not to scale.

B. UF NIT

A schematic of the UF NIT is shown in Figure 2. The cross-section of the waveguide is 25.4 mm by 25.4 mm, which provides a usable frequency range of 0.5 to 6.7 kHz. The acoustic pressure signals are measured using Brüel and Kjær Type 4138 microphones and a Brüel and Kjær Pulse Analyzer data acquisition system. The excitation signal originates from the Pulse Analyzer, is amplified by a Techron Model 7540 power amplifier, and is applied to a BMS H4590P compression driver.

The ambient gas temperature is measured using a surface-mounted platinum resistive thermal device (Omega SRTD-1). Multiple readings are averaged to estimate the temperature in the tube. The measurement microphones are flush mounted in a rotating plug that allows for convenient and precise switching of the microphone locations. The microphone location closest to the specimen with its 95% confidence interval estimate is located 32.0 ±0.8 mm from the specimen. The spacing between the two microphones with its 95% confidence interval estimate is 20.7 ± 1.1mm.

The two excitation signals chosen for the measurements are a single-tone sine wave and a white noise signal. The single-tone sine wave signal is used as a control to measure the acoustic impedance of the sample without influence from other frequencies but requires more time to conduct the full measurement as compared to the broadband excitation source. The sound pressure level at the reference microphone is set to $120\,dB$ (note that all decibel units are referenced to $20\,\mu Pa$) for each frequency. The measurement is repeated at each frequency starting from 500 Hz to 3 kHz in steps of 100 Hz. The unweighted partial overall sound pressure level (obtained by integrating from 500 Hz to 3 kHz) at the reference microphone is again set to $120\,dB$ for the white noise signal. For both excitation signals the microphone signals are acquired and processed using discrete Fourier Transform techniques. All data are acquired in the frequency range from 500 Hz to 3 kHz with a resolution of 25 Hz. A center of a frequency bin is exactly matched to the frequency of the excitation signal for the single-tone sine wave measurements. For the white noise excitation, a Hanning window with 75% overlap is used to minimize leakage.

C. NASA NIT

The data used in the current study are acquired in a normal incidence tube (NIT) located in the Flow Impedance Test Laboratory of NASA Langley Research Center. A schematic illustrating this apparatus is shown in Figure 3. The tube has a cross-section of 50.8 mm by 50.8 mm, a length of 610 mm, which provides a usable frequency range of 0.5 to 3.0 kHz. The acoustic pressure signals are measured using 6.35 mm-diameter condenser-type microphones and an Ono-Sokki FFT analyzer. Six 120-watt acoustic drivers are combined via a manifold to generate acoustic plane waves over the usable frequency range. The measurement microphones are flush mounted in a rotating plug that allows for convenient and precise switching of the microphone locations. The spacing between the two microphones is 31.75 mm.

The two excitation signals chosen for the measurements are a single-tone sine wave and a white noise signal. The sound pressure level at the reference microphone is set to $120\,dB$ for each frequency. The measurement is repeated at each frequency starting from 500 Hz to 3 kHz in steps of 100 Hz. The unweighted partial overall sound pressure level (as integrated from 500 Hz to 3 kHz) at the reference microphone is again set to $120\,dB$ for the white noise signal. For both excitation signals the microphone signals are acquired and processed using discrete Fourier Transform techniques. The data are acquired in the frequency range from 500 Hz to 3 kHz with a resolution of 25 Hz. A center of a frequency bin is exactly matched to the frequency of the excitation signal for the single-tone sine wave measurements. For the white noise excitation, a Hanning window with greater than 50% overlap is used to minimize leakage.

IV. Experimental Results

The measured data from both normal-incidence impedance tubes are presented in this section. First the single-tone sine wave data are presented, followed by the broadband data.

A. Single-tone Data

The ten individual measurements from the UF NIT for the single-tone sine wave source, and the normalized acoustic impedance model prediction results are shown in Figure 4. The figure shows that most of the variation in the normalized acoustic impedance between the ten individual samples is near anti-resonance, in particular the 2.2 and 2.3 kHz test tones. At anti-resonance, the normalized reactance of the sample is zero. Furthermore, the specific acoustic impedance is real and large so the particle velocity is small. In contrast, at resonance, the acoustic reactance also vanishes, but the acoustic resistance is small so the particle velocity at resonance has a large amplitude. Figure 5 displays the single-tone sine wave data for the NASA NIT, and the prediction. These data again have the most variability at anti-resonance and appear to have an outlier present that is easily seen in the normalized resistance at a frequency of 2.2 kHz. This data point is confirmed to be an outlier by the use of the Fast-MCD method for outlier detection [17]. Thus these sample data are removed from the NASA NIT data set for the remainder of this analysis. For both cases, the normalized acoustic impedance model matches the data reasonably well and captures greater detail than is present in the single tone data. The broadband data source in the next section

provides improved frequency resolution and constitutes a more rigorous comparison to the analytical impedance model.
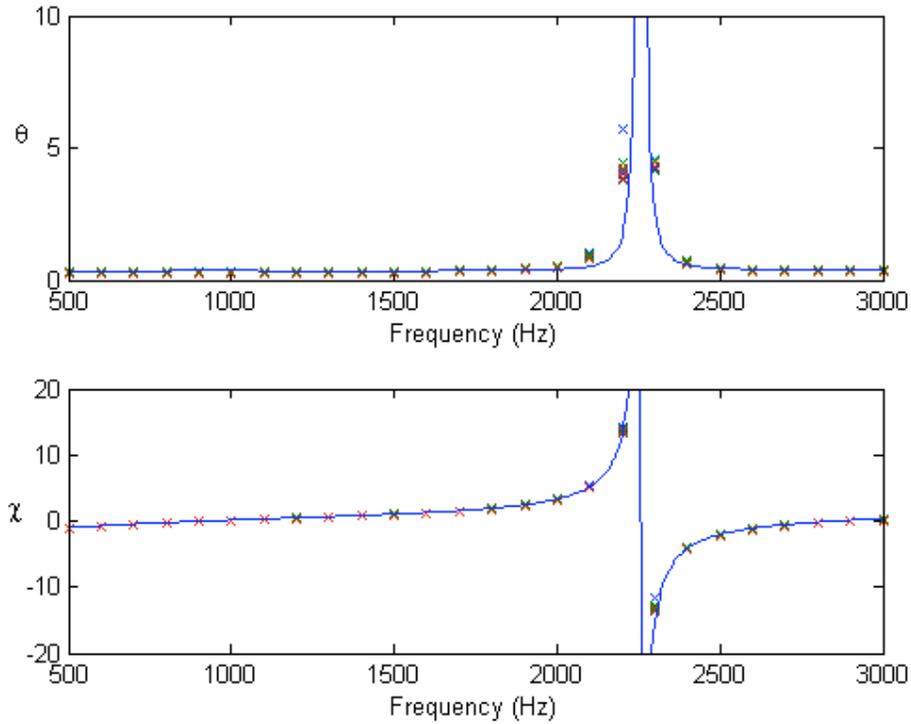
Figure 4. Comparison between normalized acoustic impedance results (symbols) from the UF NIT for the ten samples tested with a single-tone source at a sound pressure level of 120 dB and the prediction (solid-line).
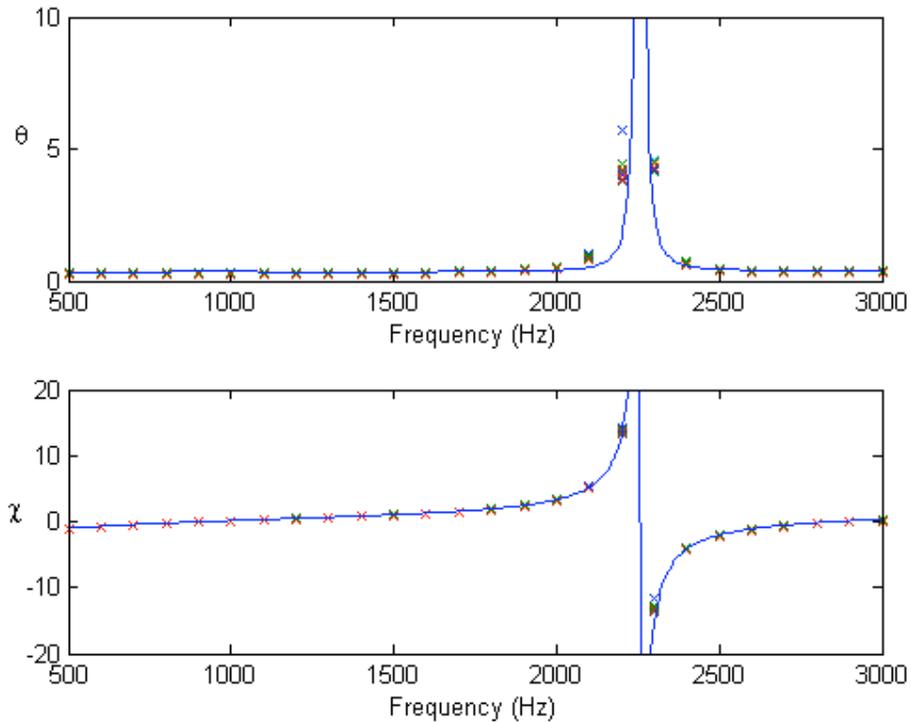
Figure 5. Comparison between normalized acoustic impedance results (symbols) from the NASA NIT for the ten samples tested with a single-tone source at a sound pressure level of 120 dB and the prediction (solid-line).

The comparison between the mean of the UF NIT dataset and the mean of the NASA NIT dataset is shown in Figure 6 for the single-tone excitation. The two experimental estimates for the normalized acoustic impedance compare favorably except at anti-resonance. In particular, the UF NIT estimate for the normalized resistance is more than twice that of the NASA NIT estimate at 2.3 kHz, and the UF estimate for the normalized reactance at 2.2 kHz is approximately 27% larger than the NASA estimate.
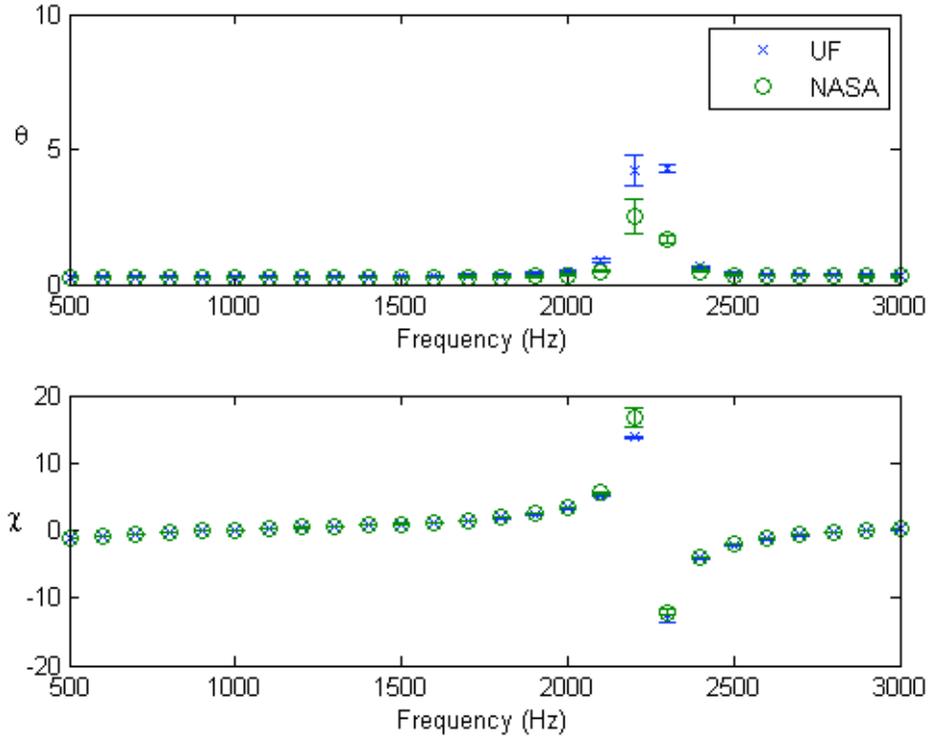
Figure 6. Comparison between UF and NASA mean normalized acoustic impedance results with a single-tone source at a sound pressure level of 120 dB. The error bars represent the sample standard deviation for each data set. Sample 9 from the NASA NIT results are removed as an outlier.

B. Broadband Data

The ten individual measurements for the broadband source for the UF NIT and the theoretical prediction are shown in Figure 7, and the NASA NIT results and the normalized acoustic model estimation are shown in Figure 8. Again, most of the variation is found at the anti-resonance frequency of the specimen, with the NASA NIT results showing greater variability. For example, the maximum value of the normalized resistance varies from 44.1 to 49.3 for the UF NIT data, whereas the NASA NIT data varies from 19.1 to 44.0. It should be noted that the scale for normalized resistance is much larger for the broadband data than for the single-tone data. This is primarily due to the frequency resolution of each acquisition. The broadband data are acquired with much finer frequency resolution, 25 Hz as compared to 100 Hz, and thus are able to capture the peaks near anti-resonance.

The comparison between the mean of the UF NIT dataset and the mean of the NASA NIT dataset for a broadband source is shown in Figure 9. The two estimates for the normalized acoustic impedance compare favorably except at anti-resonance. In particular, the UF average estimate for the normalized resistance at 2.25 kHz is approximately 64% larger than the NASA average estimate. Also, the frequencies of the maximum and minimum normalized reactance values are 2.225 kHz and 2.25 kHz for the NASA NIT and 2.225 kHz and 2.275 kHz for the UF NIT.

The sample-to-sample standard deviations of the normalized resistance and reactance are computed separately for the UF and NASA data sets to further compare the facilities and sample size. The standard deviations are displayed in two ways, one with absolute units shown in Figure 10 and one with relative units shown in Figure 11. The graphs show that UF NIT dataset has less variation around the anti-resonance but more variation elsewhere. The covariance between the normalized resistance and normalized reactance for both the UF NIT dataset and the NASA NIT dataset is between ±0.01 for all frequencies except for the anti-resonance frequency and adjacent bins

8

American Institute of Aeronautics and Astronautics

where the absolute value of the covariance increases. The low value for the covariance indicates the normalized resistance and reactance are not linearly correlated.

A Monte Carlo simulation is performed on the UF dataset to evaluate the amount of uncertainty in the mean estimate for the normalized acoustic impedance data. The Monte Carlo simulation is performed by saving the raw statistical results of the Monte Carlo simulation used to produce the UF uncertainty estimates for each individual sample as described in [12]. The 40,000 Monte Carlo estimates for the normalized acoustic impedance for each individual sample as a function of frequency are then used to produce 40,000 estimates the mean normalized acoustic impedance for the UF dataset as a function of frequency. These estimates represent an approximation to the probability distribution of the mean estimate for the acoustic impedance due to the uncertainty of each input or individual sample. The data are then used to compute statistical quantities such as the standard deviation and the covariance. The standard deviation of the resistance and reactance are shown in Figure 12 with absolute units and in Figure 13 with relative units. The results are compared to the sample-to-sample variation, quantified by the standard deviation, shown in Figures 10 and 11. On inspection, the two different sources of variation are similar in order of magnitude and thus both sources of variation must be accounted for when estimating the total variation in the mean estimate for the acoustic impedance of the liner.
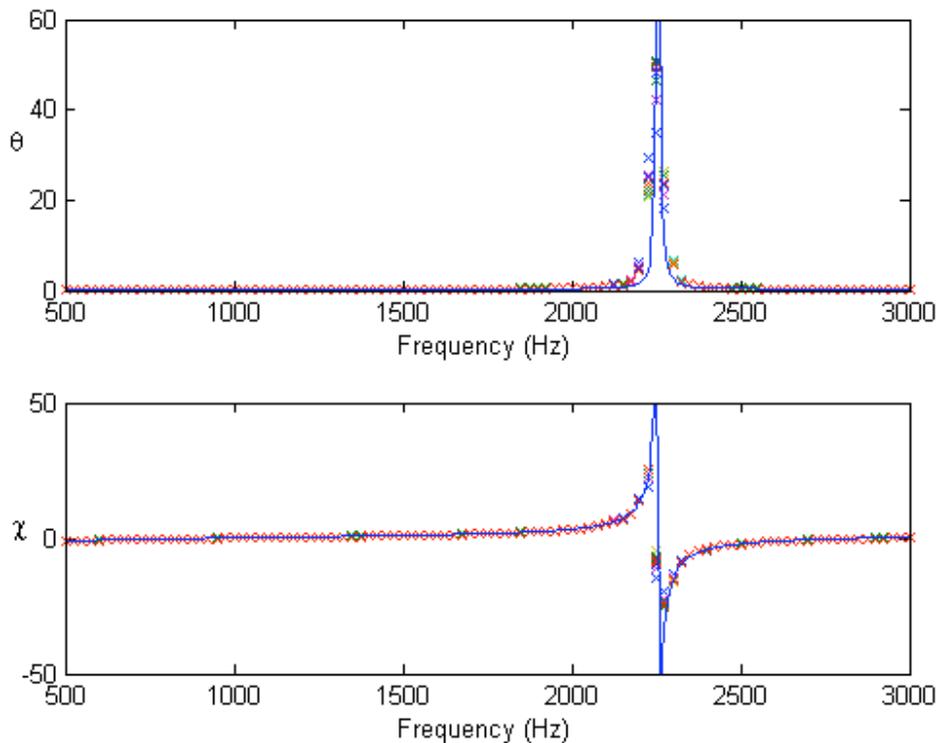
Figure 7. Comparison between normalized acoustic impedance results (symbols) from the UF NIT for the ten samples tested with a broadband source at an overall sound pressure level of 120 dB and the prediction (solid line).

American Institute of Aeronautics and Astronautics
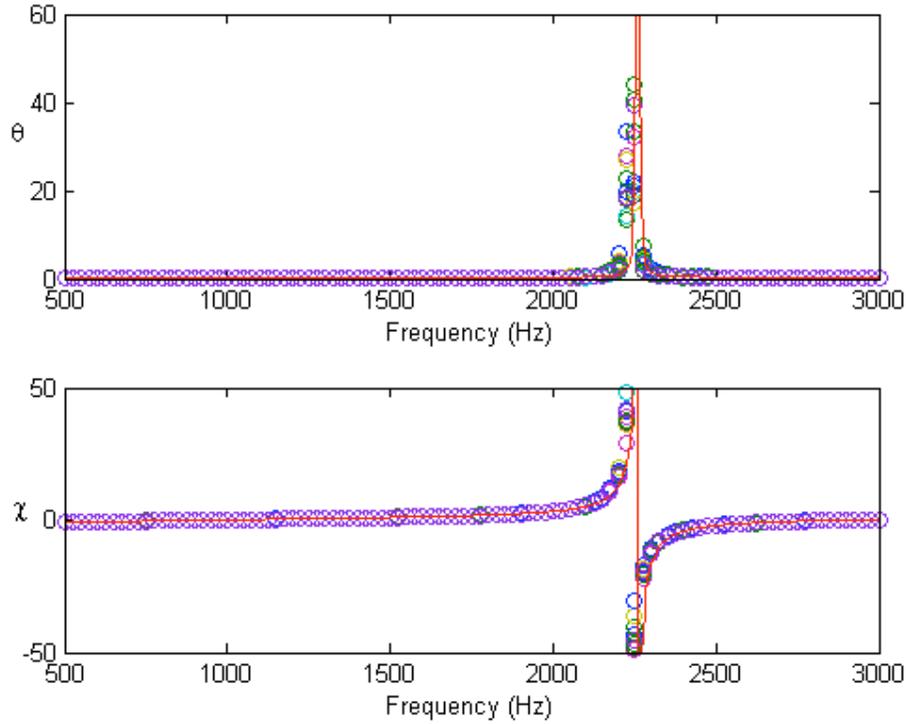
Figure 8. Comparison between normalized acoustic impedance results (symbols) from the NASA NIT for the ten samples tested with a broadband source at an overall sound pressure level of 120 dB and the prediction (solid line).
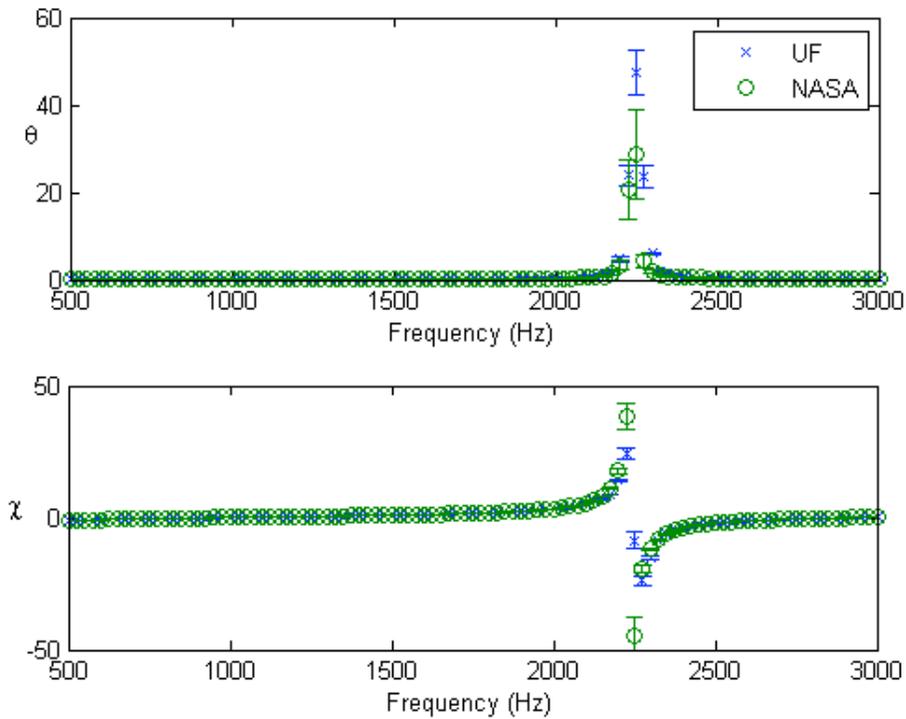
Figure 9. Comparison between UF and NASA mean normalized acoustic impedance results with a broadband source at a sound pressure level 120 dB.
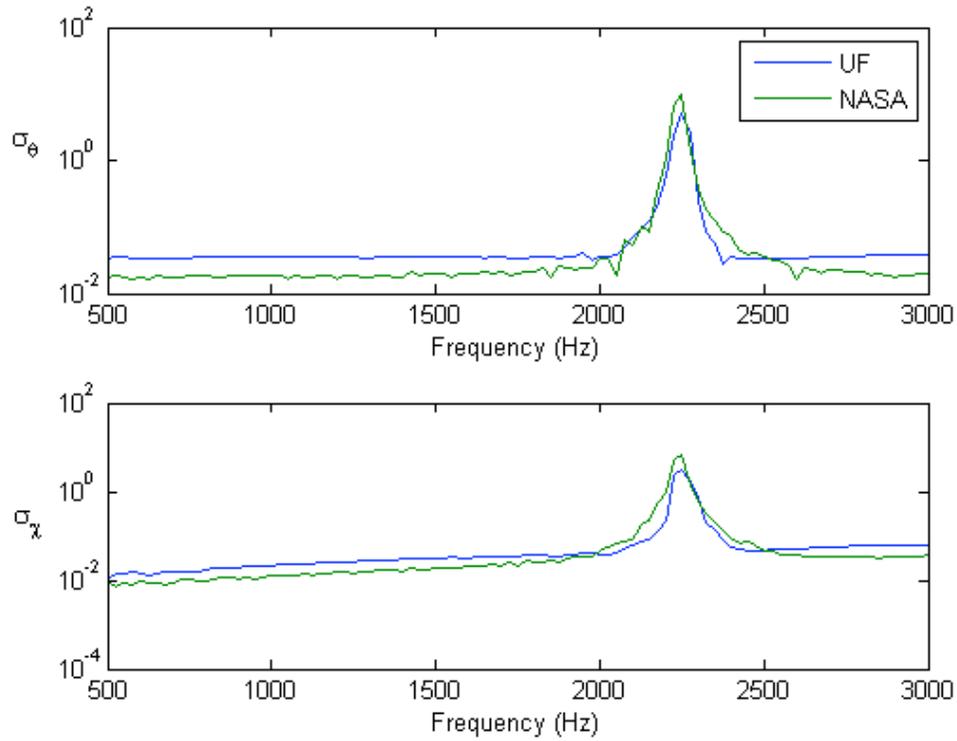
Figure 10. Comparison between the standard deviation of the UF dataset and the NASA dataset for the broadband source at a sound pressure level of 120 dB displayed in absolute units.
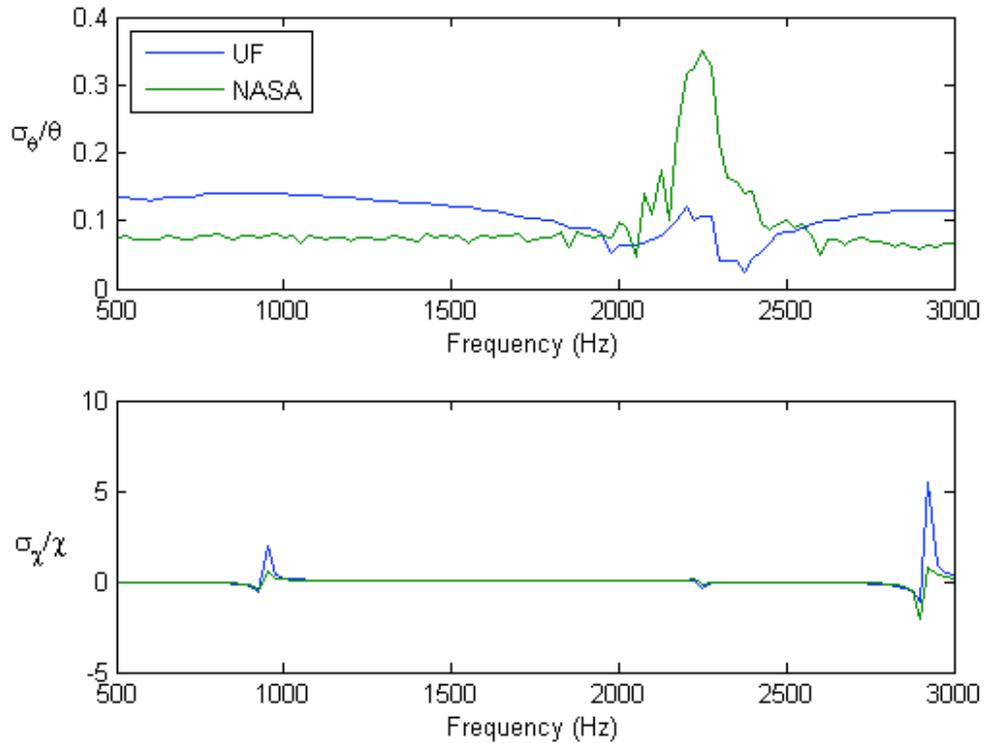
Figure 11. Comparison between the standard deviation of the UF dataset and the NASA dataset for the broadband source at a sound pressure level of 120 dB displayed in relative units.

American Institute of Aeronautics and Astronautics
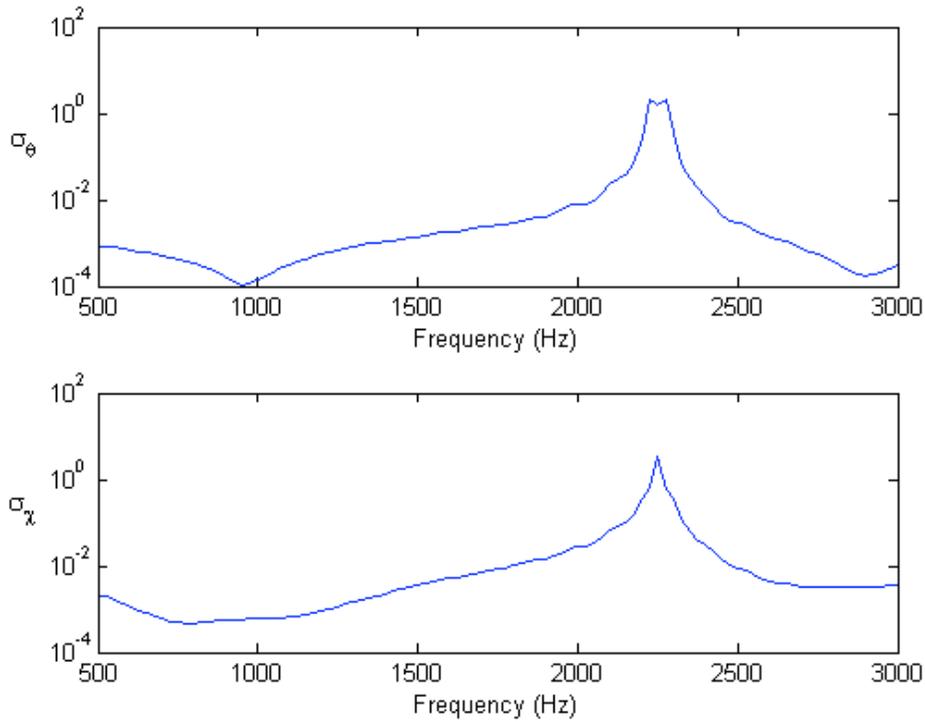
Figure 12. The standard deviation of the UF dataset calculated from the results of the Monte Carlo simulation for the broadband source at a sound pressure level of 120 dB displayed in absolute units.
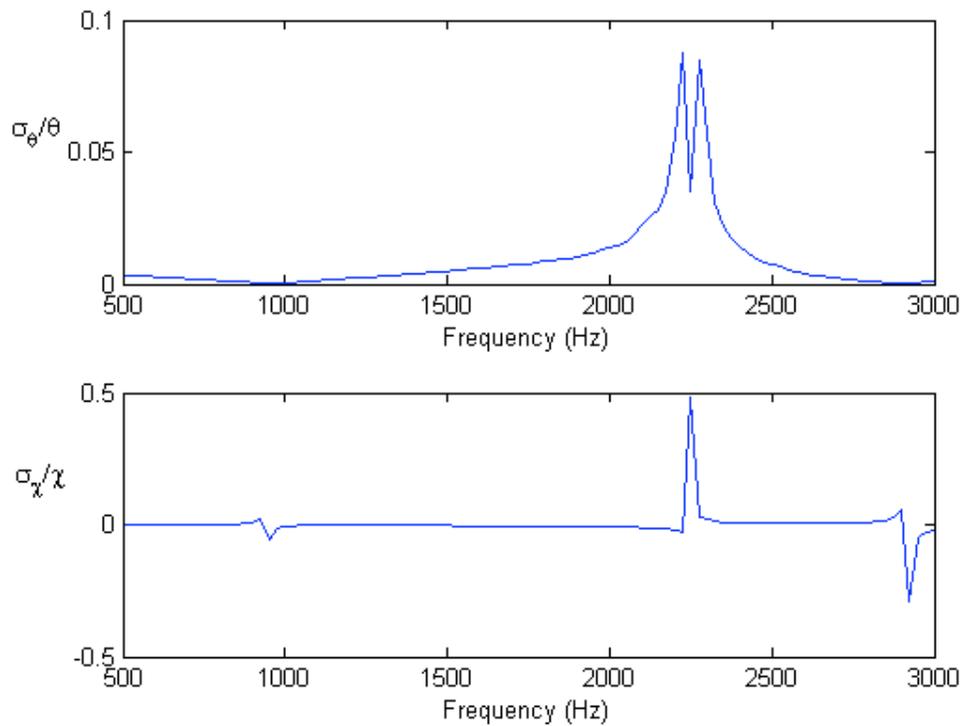
Figure 13. The standard deviation of the UF dataset calculated from the results of the Monte Carlo simulation for the broadband source at a sound pressure level of 120 dB displayed in ralative units.

American Institute of Aeronautics and Astronautics

V. Conclusions

The results from the UF NIT and the NASA NIT data sets show that the two facilities are quantitatively similar, but the results for the NASA estimates vary significantly from the UF results near anti-resonance. Possibly, this discrepancy is due to cross-sectional area-dependent cavity dissipation. This suggests improvements can be made on the procedures to reduce the variability from facility to facility. Investigation of the effect of the facility on the measurement and the estimation of the confidence intervals for all measurements could allow better comparison between facilities. The results of this study prevent us from definitively stating whether the acoustic impedance estimates from the two facilities agree or disagree with each other due to the lack of uncertainty information for the NASA data. This study also demonstrated that the total variation of the mean estimate of the acoustic impedance from the ten individual samples must consider the two sources of variation, the variation from sample to sample and the uncertainty of the measurement of each individual sample estimate, since both are on the same order of magnitude. Therefore the individual uncertainty estimates are needed to definitely state whether or not the results from the two facilities are statistically in agreement. The results show the most visible variation at the anti-resonance frequency and also exhibit substantial sample-to-sample variations. Overall, the sample variations are comparable in magnitude to the facility deviations, thus supporting the notion that the difference in sample size, 25.4 mm for the UF NIT and 50.8 mm for the NASA NIT, does not significantly impact the measured acoustic impedance. Thus, a sample 25.4 mm by 25.4 mm is representative of the overall material for the specific single degree-of-freedom liner tested in this study.

Acknowledgments

References

1. Motsinger, R.E. and R.E. Kraft, Design and performance of duct acoustic treatments, in: H.H. Hubbard (Ed.), *Aeroacoustics of Flight Vehicles: Theory and Practice Volume 2: Noise Control*, Acoustical Society of America: New York, 1995, pp. 165-206.
2. ASTM-E1050-98, *Impedance and Absorption of Acoustical Materials Using a Tube, Two Microphones and Digital Frequency Analysis System*. 1998, ASTM International.
3. Chung, J.Y. and D.A. Blaser, Transfer function method of measuring in-duct acoustic properties, I-Theory, II-Experiment. *Journal of the Acoustical Society of America* 68(3) (1980) 907-921.
4. ISO-10534-2:1998, *Acoustics-Determination of Sound Absorption Coefficient and Impedance in Impedance Tubes: Part 2: Transfer-function method*. 1998: International Organization for Standardization.
5. Jones, M.G. and T.L. Parrott, Evaluation of a multi-point method for determining acoustic impedance. *Mechanical Systems and Signal Processing* 3(1) (1989) 15-35.
6. Jones, M.G. and P.E. Stiede, Comparison of methods for determining specific acoustic impedance. *Journal of the Acoustical Society of America* 101(5) (1997) 2694-2704.
7. Åbom, M. and H. Bodén, Error analysis of two-microphone measurements in ducts with flow. *Journal of the Acoustical Society of America* 83(6) (1988) 2429-2438.
8. Bodén, H. and M. Åbom, Influence of errors on the two-microphone method for measuring acoustic properties in ducts. *Journal of the Acoustical Society of America* 79(2) (1986) 541-549.
9. Seybert, A.F. and B. Soenarko, Error analysis of spectral estimates with application to the measurement of acoustic parameters using random sound fields in ducts. *Journal of the Acoustical Society of America* 69(4) (1981) 1190-1199.
10. Katz, B.F.G., Method to resolve microphone and sample location errors in the two-microphone duct measurement method. *Journal of the Acoustical Society of America* 108(5) (2000) 2231-2237.
11. Schultz, T., *Acoustic Impedance Testing for Aeroacoustic Applications*, in *Mechanical and Aerospace Engineering*. 2006, University of Florida: Gainesville, FL.
12. Schultz, T., M. Sheplak, and L. Cattafesta, Uncertainty analysis of the two-microphone method. *Journal of Sound and Vibration* 304 (2007) 91-109.
13. Crandall, I. B., *Theory of Vibrating Systems and Sound* , D. Van Nostrand Company ,New York, 1926, pp. 229–241.
14. Melling, T. H., The acoustic impedance of perforates at medium and high sound pressure levels. *Journal of Sound and Vibration* 29 (1973), 1–65.
15. Rechevkin. S.N., A *Course of Lectures on the Theory of Sound*. Pergamon Press, London, 1963.

16.   Blackstock, D.T., Fundamentals of Physical Acroustics, John Wiley & Sons, Inc. New York, 2000
17.   Parrott, T.L. and Jones, M.G., "Cascaded Perforates as One-Dimensional, Bulk Absorbers," AIAA-2006-2402 , 12th AIAA/CEAS Aeroacoustics Conference (27th AIAA Aeroacoustics Conference), Cambridge,